Microelectronics Reliability 52 (2012) 1532–1538

Contents lists available at SciVerse ScienceDirect

Microelectronics Reliability

journal homepage: www.elsevier.com/locate/microrel

Interconnect reliability dependence on fast diffusivity paths

Hajdin Ceric [a,b,*], Roberto Lacerda de Orio [a,b], Siegfried Selberherr [b]

[a] Christian Doppler Laboratory for Reliability Issues in Microelectronics, TU Wien, Gußhausstraße 27–29/E360, A-1040 Wien, Austria
[b] Institute for Microelectronics, TU Wien, Gußhausstraße 27–29/E360, A-1040 Wien, Austria

ARTICLE INFO

Article history:
Received 12 August 2011
Received in revised form 23 September 2011
Accepted 27 September 2011
Available online 1 November 2011

ABSTRACT

The reliability of interconnects in modern integrated circuits is determined by the magnitude and direction of the effective valence for electromigration (EM). The effective valence depends on local atomistic configurations of fast diffusivity paths such as metal interfaces, dislocations, and the grain boundary; therefore, microstructural variations lead to a statistically predictable behavior for the EM life time. Quantum mechanical investigations of EM have been carried out on an atomistic level in order to obtain numerically efficient methods for calculating the effective valence. The results of *ab initio* calculations of the effective valence have been used to parametrize the continuum-level EM models. The impact of fast diffusivity paths on the long term EM behavior is demonstrated with these models.

1. Introduction

Extensive EM experiments have produced an ample amount of data, indicating that the copper interconnect life time has decreased for every new interconnect generation, even when tested at the same current density [1]. Newer interconnects, due to their reduced size, require a smaller void volume for failure and a larger fraction of atoms is transferred, along the fast interface, to the capping layer and the grain boundary diffusion paths. The bamboo-like copper grain structure, observed in interconnects above the 65 nm technology node, does not exist in interconnects below the 65 nm node, where line sections of the polycrystalline grain structure dominate.

The improvement of the EM behavior for the 22 nm technology node and beyond faces a new challenge, because this EM-induced mass transport increasingly depends on the copper microstructure and the interface properties related to the fabrication conditions [2]. Improving the overall interconnect reliability can only be achieved with a combination of different techniques, such as copper alloying, thicker liner, large via size, embedded via, and strengthening of the copper/dielectric interface.

Modern Technology Computer-Aided Design (TCAD) tools, in order to meet the challenges of contemporary interconnects, must cover two major areas: physically based continuum-level modeling and first-principle/atomistic-level modeling. A multilevel modeling and simulation approach is presented in order to investigate the impact of fast diffusivity paths on EM reliability.

2. Fast diffusivity paths

2.1. Grain boundaries

Since atoms are more loosely bound at grain boundaries than in the lattice, atoms migrate along grain boundaries more easily than through the lattice. Therefore, the EM failure rate should depend on the grain size of the metallic thin film. Such a dependence is well documented for aluminum interconnects, however, the dependence is found to be less pronounced in copper interconnects. The reason is probably that EM along interfaces is dominant in copper interconnects. However, the difference in EM performance between interconnect lines with large and small grains can clearly be seen. Electroplated copper in dual-damascene structures has significantly larger grains than CVD copper lines resulting in a longer EM life time [3].

2.2. The etch stop/copper interface

The interface between copper and the capping layer is known to be the dominant diffusion pathway in dual-damascene interconnects [4]. The properties of this particular interface play therefore a key role for EM. SiN- and SiC-based films are widely used as capping materials for copper interconnects. It has been shown in several studies [5] that the EM life time depends on the adhesion behavior, i.e. the sticking coefficient between the capping layer and the copper surface. Good adhesion and hence large EM life times are enabled by a tightly bonded interface which suppresses the migration along this pathway. Recently, numerous experiments have shown that the best results are obtained, when an adherent metallic layer, such as electroless CoWP, is applied to the surface before deposition of the interlevel dielectric. In such

* Corresponding author at: Christian Doppler Laboratory for Reliability Issues in Microelectronics, Institute for Microelectronics, TU Wien, Gußhausstraße 27–29/E360, A-1040 Wien, Austria. Tel.: +43 1 58801 36032; fax: +43 1 58801 36099.
E-mail address: Ceric@iue.tuwien.ac.at (H. Ceric).

0026-2714/$ - see front matter © 2011 Elsevier Ltd. All rights reserved.
doi:10.1016/j.microrel.2011.09.035

a case, a thin (~10 nm) layer is sufficient to completely stop all interfacial diffusion.

3. Continuum-level modeling

Several driving forces are responsible for the vacancy transport in a conductor line under EM. The combination of these driving forces leads to the total vacancy flux given by [6]

$$\vec{J}_v = -D_v\left(\nabla C_v + \frac{|Z^*e|}{k_BT}C_v\nabla\varphi + \frac{f\Omega}{k_BT}C_v\nabla\sigma\right), \quad (1)$$

where D_v is the vacancy diffusion coefficient of the dominant transport path, C_v is the vacancy concentration, Z^*e is the effective charge, f is the vacancy relaxation ratio, Ω is the atomic volume, σ is the hydrostatic stress, k_B is Boltzmann's constant, T is the temperature, and φ is the electric potential. A closer look at Eq. (1) reveals that the three major driving forces which induce the dynamics of vacancies are: the electromigration which is proportional to $\nabla\varphi$, the concentration gradient ∇C_v, and the mechanical stress gradient $\nabla\sigma$.

Vacancies accumulate or vanish in sites of flux divergence, and this dynamics is described by the vacancy balance equation

$$\frac{\partial C_v}{\partial t} = -\nabla\cdot\vec{J}_v + G(C_v), \quad (2)$$

where $G(C_v)$ is the source function which models vacancy generation and annihilation processes.

4. Modeling of grain boundaries

The grain boundary is treated as a separate medium with the capability of absorbing and releasing vacancies. Vacancies are trapped from both neighboring grains with a trapping rate ω_T and released to these grains with a release rate ω_R.

The vacancy concentration from both sides of the grain boundary is denoted as C_v^1 and C_v^2. Correspondingly, the fluxes are calculated as

$$J_{v,1} = \omega_T\left(C_v^{eq} - C_v^{im}\right)C_v^1 - \omega_R C_v^{im}, \quad (3)$$

$$-J_{v,2} = \omega_T\left(C_v^{eq} - C_v^{im}\right)C_v^2 - \omega_R C_v^{im}. \quad (4)$$

The vacancies are captured at the grain boundary and converted into immobile vacancies $\left(C_v^{im}\right)$. This is mathematically expressed as

$$\frac{\partial C_v^{im}}{\partial t} = \frac{J_{v,1} - J_{v,2}}{\delta} = -\left(\frac{\partial C_v^1}{\partial t} + \frac{\partial C_v^2}{\partial t}\right), \quad (5)$$

where δ is the grain boundary thickness. By combining Eqs. (3)–(5) with the vacancy balance Eq. (2), the following equation is obtained:

$$\frac{\partial C_v^\alpha}{\partial t} = -\mathrm{div}\vec{J}_{v,\alpha} + \frac{1}{\tau}\left(C_v^{eq} - C_v^{im}\left(1 + \frac{2\omega_R}{\omega_T\left(C_v^1 + C_v^2\right)}\right)\right), \quad (6)$$

$\alpha = 1$ and $\alpha = 2$ indicate the left and the right side of the grain boundary, respectively. $\vec{J}_{v,\alpha}$ is the vacancy transport driven by EM and a stress gradient. τ is expressed by

$$\frac{1}{\tau} = \frac{\omega_T\left(C_v^1 + C_v^2\right)}{\delta}. \quad (7)$$

The capacity of the grain boundary to accept trapped vacancies is expressed by the stress-dependent equilibrium concentration [6,7]

$$C_v^{eq} = C_v^0\exp\left(\frac{\sigma_{nn}\Omega}{k_BT}\right), \quad \sigma_{nn} = \vec{n}\cdot\bar{\bar{\sigma}}\cdot\vec{n}, \quad (8)$$

where we assume a unique equilibrium vacancy concentration C_v^0 in stress free copper, in the grain's bulk, and in the grain boundaries. $\vec{n}$ is the normal vector to the grain surface and $\bar{\bar{\sigma}}$ is the stress tensor.

The full description of the atomic mechanisms of vacancy generation and annihilation (e.g. determination of parameters ω_T and ω_R) in grain boundaries goes beyond the capability of continuum-level modeling and can only be obtained by molecular dynamics methods.

5. Atomistic-level modeling

The description of grain boundaries in the framework of continuum-level modeling is ultimately incomplete too, because the crucial parameter to determine the EM behavior, the effective valence, can be reliably obtained experimentally only for the bulk of metals. Extending experimental methods for grain boundaries and interfaces demands additional, often questionable assumptions [8].

In general, the effective valence is a tensor field ($\bar{Z}$), defined as a linear relationship between the EM force ($\vec{F}$) and an external electric field $\vec{E}$.

$$\vec{F}(\vec{R}) = e\bar{Z}(\vec{R})\vec{E} \quad (9)$$

Using the Born–Oppenheimer approximation, the force, $F(\vec{R})$, exerted by the electron gas on an atom situated at $\vec{R}$, may be written as [9–11]

$$F(\vec{R}) = \sum_{\vec{k}} g(\vec{k})\langle\psi_{\vec{k}}(\vec{r})|-\nabla_{\vec{R}}V(\vec{r}-\vec{R})|\psi_{\vec{k}}(\vec{r})\rangle, \quad (10)$$

where V is the interaction potential between an electron and the migrating atom, $\psi_k(\vec{r})$ are the scattering states for electrons in the absence of an external electric field, and $g(\vec{k})$ is the shifted electron distribution which has the form

$$g(\vec{k}) = e\tau(\vec{k})\vec{v}(\vec{k})\cdot\vec{E}\frac{\partial f_0}{\partial\mathcal{E}_{\vec{k}}}. \quad (11)$$

Here f_0 is the equilibrium electron distribution, $\tau(\vec{k})$ is the relaxation time due to scattering by phonons, and $v(\vec{k})$ is the electron group velocity. In the low temperature limit

$$\frac{\partial f_0}{\partial\mathcal{E}_{\vec{k}}} = -\delta(\mathcal{E}_F - \mathcal{E}_{\vec{k}}) \quad (12)$$

and (10) is then re-written in the form

$$\vec{F}(\vec{R}) = \frac{e\Omega}{4\pi^3}\iiint d^3\vec{k}\,\delta(\mathcal{E}_F - \mathcal{E}_{\vec{k}})\tau(\vec{k})[\vec{v}(\vec{k})\cdot\vec{E}] \cdot \iiint_{EZ} d^3\vec{r}\,\psi_k^*(\vec{r})\nabla_{\vec{R}}V(\vec{R}-\vec{r})\psi_k(\vec{r}). \quad (13)$$

Ω is the volume of a unit cell. The first integration is over the k-space and the second over the volume of the crystal. By taking into account (9) and

$$\rho(\vec{k},\vec{r}) = |\psi_k(\vec{r})|^2 \quad (14)$$

the components of the effective valence tensor $\bar{Z}$ are expressed as

$$Z_{i,j}(\vec{R}) = \frac{\Omega}{4\pi^3}\iiint d^3\vec{k}\,\delta(\mathcal{E}_F - \mathcal{E}_{\vec{k}})\tau(\vec{k})[\vec{v}(\vec{k})\cdot\hat{x}_j] \cdot \iiint d^3\vec{r}\,\rho(\vec{k},\vec{r})\left[\nabla_{\vec{R}}V(\vec{R}-\vec{r})\cdot\hat{x}_i\right], \quad i,j = x,y. \quad (15)$$

For the calculation of the electron density the DFT tool VASP [12] was used. The electron density alone provides a qualitative explanation for the fact that the effective valence is higher in the bulk than in the grain boundaries. Similar analyses can be performed for

atomic structures of different copper/insulator interfaces. Higher electron densities lead to higher effective valences, as can be seen from (15).

The electric potential calculated with DFT is also applied for a simple jellium model. Here, the grain boundary is represented as a repulsive potential barrier for current carrying electrons. In this case the evaluation of integral (15) is not necessary, since only a simple one-dimensional barrier problem must be dealt with, e.g. the precisely calculated DFT repulsive potential is approximated with a rectangular barrier potential. To estimate the value of the effective valence, both, inside the grain boundary and in the copper bulk, an external electric field parallel to the grain boundary must be applied, obtaining the two-dimensional potential. Current carrying electrons are now described with the two-dimensional Schrödinger equation.

The electron density $\rho(\vec{r})$ is easily calculated by integrating over the continuous energy states.

$$\rho(\vec{r}) = \int_0^\infty f(\mathcal{E} - \mathcal{E}_F) DOS(\mathcal{E}) |\psi(x, y; \mathcal{E})|^2 d\mathcal{E} \tag{16}$$

Now, the electron wind force is given by a simpler expression [13]

$$\overrightarrow{F}(\overrightarrow{R}) = -\int \rho(\vec{r}) \frac{\partial V(\vec{r} - \overrightarrow{R})}{\partial \overrightarrow{R}} d^3 r, \tag{17}$$

which is subsequently used in order to calculate the effective valence.

The electric potential inside the bulk and the grain boundary is calculated by means of DFT (cf. Fig. 1). Additionally the Fermi energy has been determined. The one-dimensional distribution of the effective valence is shown in Fig. 2. According to our calculation the effective valence inside the grain boundary is found to be 75% lower than in the bulk for a Fermi energy of 4.3 eV, a value which is in good agreement with the calculation of Sorbello [14].

In Fig. 3 we show characteristic curves of the EM related vacancy concentration build-up for an extended simulation time. Here a parametrized continuum-level EM model is used [6]. All three curves are obtained for the same layout and operating conditions, but they differ because of a different copper microstructure.

6. Fast diffusivity paths and void evolution

When a sufficiently high stress level is reached at some interfacial spot, where a flaw can be assumed, the failure development enters the next phase and a different modeling ansatz must be applied. Here, we have an evolving void surface shaped by two dynamic forces: the chemical potential gradient and the electron wind.

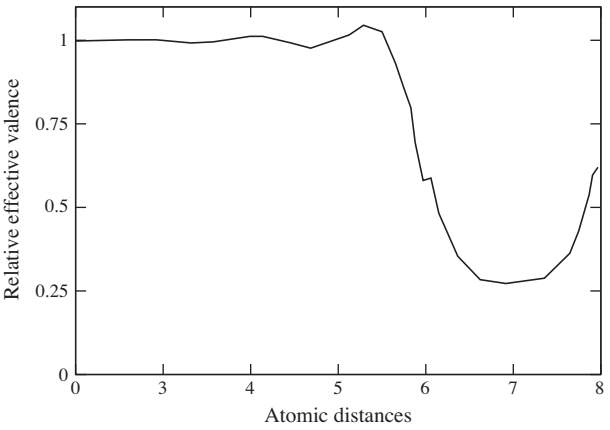

Fig. 2. Average distribution of the effective valence in x-direction near a grain boundary. The external electric field is oriented parallel to the grain boundary.

The development of fatal voids, i.e. voids which lead to a significant resistance increase, or even completely sever the line, is the ultimate cause for the EM induced interconnect failure [15]. Therefore, the understanding and prediction of EM failure behavior can only be achieved through a detailed study of the void evolution mechanisms.

Including both contributions, EM and chemical potential-driven surface diffusion, gives the total surface vacancy flux $\vec{J}_s = J_s \vec{t}$, where $\vec{t}$ is the unit vector tangential to the void surface [16]

$$\vec{J}_s = -D_s \left(eZ^* \overrightarrow{E}_s + \Omega \nabla_s \left(\frac{\bar{\bar{\sigma}} : \bar{\bar{\varepsilon}}}{2} - \gamma_s \kappa \right) \right). \tag{18}$$

$\overrightarrow{E}_s = E_s \vec{t}$ is the local component of the electric field tangential to the void surface, ∇_s is the surface gradient operator, $1/2(\bar{\bar{\sigma}} : \bar{\bar{\varepsilon}})$ is the strain energy density of the material adjacent to the void surface, and κ is the curvature of the void surface. The surface diffusivity D_s is given by an Arrhenius law

$$D_s = \frac{D_0 \delta_s}{k_B T} \exp\left(-\frac{Q_s}{k_B T} \right). \tag{19}$$

δ_s is the thickness of the diffusion layer, Q_s is the activation energy for the surface diffusion, and D_0 is the pre-exponential coefficient for mass diffusion.

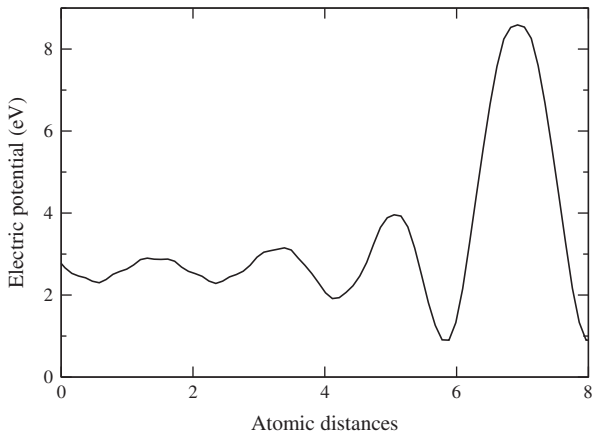

Fig. 1. Electric potential energy in the vicinity of the grain boundary and inside the grain boundary obtained by the density functional theory.

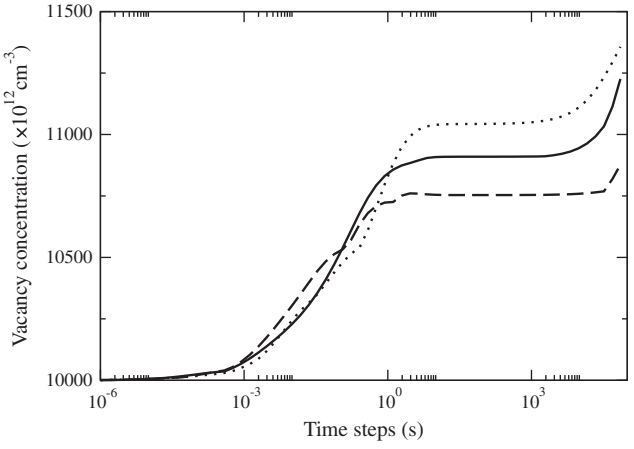

Fig. 3. Variation of the peak vacancy concentration with time for three different microstructures.

The Level-Set method is powerful for simulating moving boundary problems, where the moving boundary is implicitly represented by the level set of a given function. The time evolution of the level set is governed by a Hamilton–Jacobi equation. A velocity field, which accounts for the physical effects acting on the moving boundary, dictates the evolution of the level set. Several algorithms and strategies to implement the Level-Set method have been proposed [17].

For the case of the void surface evolving under the influence of EM and the gradient of the surface energy the Hamilton–Jacobi equation for a level set ϕ is

$$\frac{\partial \phi}{\partial t} - D_s \nabla_s \cdot \left(eZ^* \vec{E}_s - \gamma_s \Omega \nabla \cdot \left(\frac{\nabla \phi}{|\nabla \phi|} \right) \right) = 0. \tag{20}$$

The diffusion coefficient D_s has to be set according to the region, where the void surface lays. This region can be bulk, grain boundary, or the interface to capping or barrier layers. The role of the surface diffusivity variation is a potential cause for a huge diversity of void shapes which have been observed in experiments.

The site of void nucleation and the morphology of the evolving void accurately reproduce experimental observations. The simulation is started by assuming a grain boundary network (c.f. Fig. 4) in the studied dual-damascene interconnect.

The vacancy release rate ω_R and the vacancy trapping rate ω_T are chosen in such a way that during simulation the conditions

$$\frac{2\omega_R}{\omega_T \left(C_v^1 + C_v^2 \right)} \ll 1 \tag{21}$$

and

$$1\ \mathrm{s} < \tau = \frac{\delta}{\omega_T \left(C_v^1 + C_v^2 \right)} < 2\ \mathrm{s} \tag{22}$$

are fulfilled. With these conditions the model for immobile vacancies (3)–(8) behaves analogously to a classical Rosenberg–Ohring term [18], which was already successfully applied in [19], where $\tau = 1$ s and $\tau = 2$ s is used.

All parameters for our simulation are set according to experiments published in [20]. The line width is 0.18 μm, the applied current density is 1.5 MA/cm^2, and the temperature is 300 °C. Barrier and capping layer are Ta/TaN and SiCN, respectively. SiOC is used as interlayer dielectricum. The continuum Eqs. (6) are solved, until a stress threshold (σ_{th}) for void nucleation is reached at some triple point (c.f. Fig. 5). At this triple point an initial, small spherical void is set and the Hamilton–Jacobi Eq. (20) is solved.

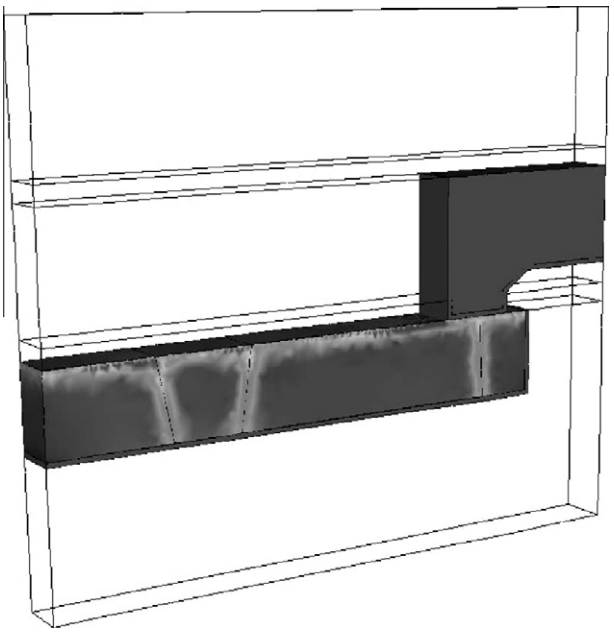

Fig. 5. Peak hydrostatic tensile stress distribution (light areas) caused by EM.

For stresses $\sigma < \sigma_{th}$ an energy barrier exists between the void embryo and a stable-growing void. If the stress is above the threshold value ($\sigma > \sigma_{th}$), the free energy monotonically decreases with the void volume, and the energy barrier vanishes. If we now assume an adhesion free patch with a radius of 10 nm (about 20 atoms), we obtain $\sigma_{th} \approx 344$ MPa [6].

After the void is nucleated at the triple point (c.f. Fig. 6), which is a natural free adhesion patch, it moves in the direction of the electric current. The void encounters the second grain boundary

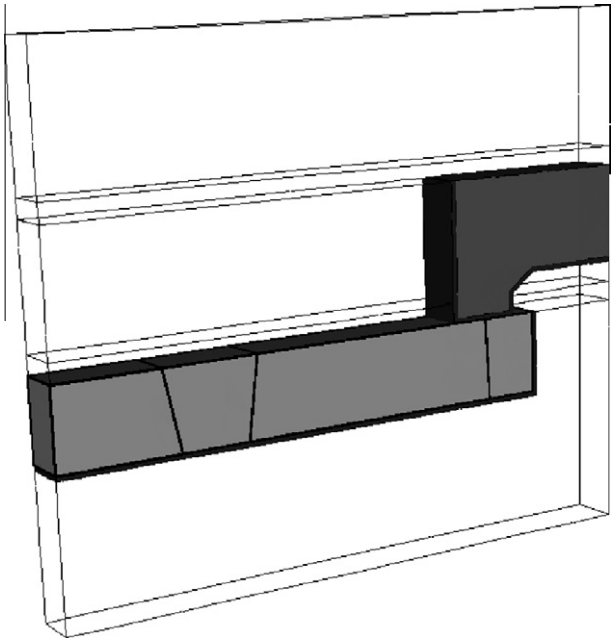

Fig. 4. Dual-damascene structure used for simulation.

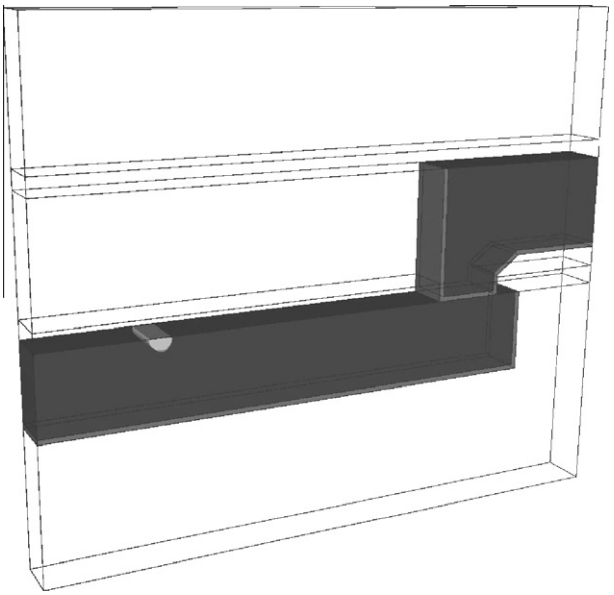

Fig. 6. Initial void placed at the nucleation site.

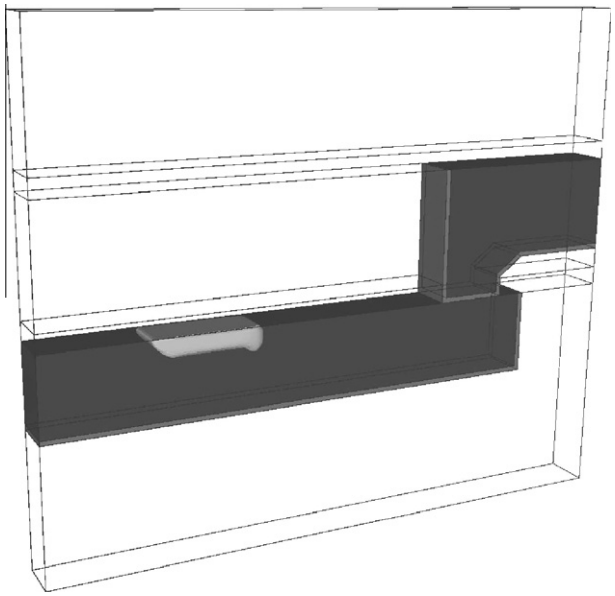

Fig. 7. The void moves and encounters the second grain boundary.

and transforms its shape (c.f. Fig. 7). During evolution the void remains attached to the copper/capping layer interface which is also a fast diffusivity path. The strength of adhesion between copper and SiCN determines the speed of the void evolution. By choosing other capping materials and corresponding technology processes which increase adhesion, the speed of the void is reduced and the interconnect life time is increased.

It can be clearly seen in Fig. 8 that the presence of a grain boundary induces a void surface movement toward the inner part of the interconnect. Here the grain boundary acts as fast diffusivity path. This result is consistent with numerous experimental observations and explains the fact that bamboo microstructures are prone to failures caused by slit-like voids [21–23].

The experimental result presented in Fig. 9 clearly shows that the applied models together with the assumed microstructure reproduce the experimentally observed void dynamics.

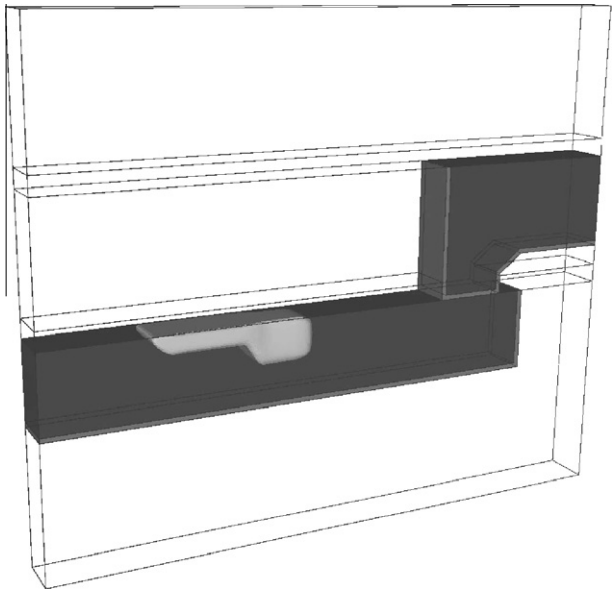

Fig. 8. The shape change is enhanced as the void drifts toward the via.

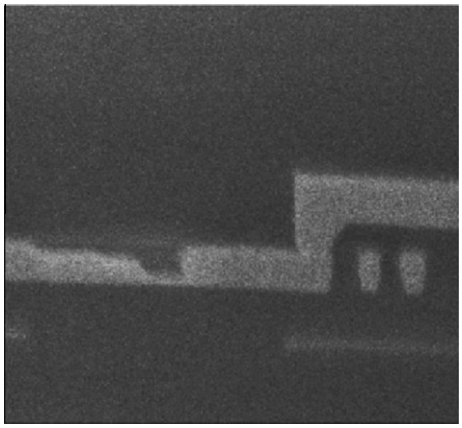

Fig. 9. FIB cross-section of interconnect after an EM test [20] (courtesy of Dr. Lucile Arnauld).

7. Statistical simulations

For a given interconnect layout and monocrystalline material, simulation will provide a unique time-to-failure. All impact factors, e.g. geometry of the layout, bulk diffusivity, interface diffusivity, and mechanical properties, are deterministic and so the time-to-failure is deterministic. However, the situation changes, when the interconnect possesses a microstructure. The microstructure has a significant impact on EM, since it introduces a diversity of possible fast EM paths and local mechanical properties (the Young modulus and Poisson factor depend on the crystal orientation in each grain).

We investigated the origin of the statistical distribution of EM times to failure as a function of the distribution of copper grain sizes. The effect of lognormal grain size distributions on the distribution of EM life times of fully three-dimensional copper dual damascene interconnect structures has been studied based on numerical simulations. We have applied a continuum-level multi-physics EM model which incorporates the effects of grain boundaries for stress build-up.

In order to include the grain distribution into the numerical simulations, a tool for microstructure generation has been developed. Given a specific interconnect structure and providing the tool with a median grain size and corresponding standard deviation, it

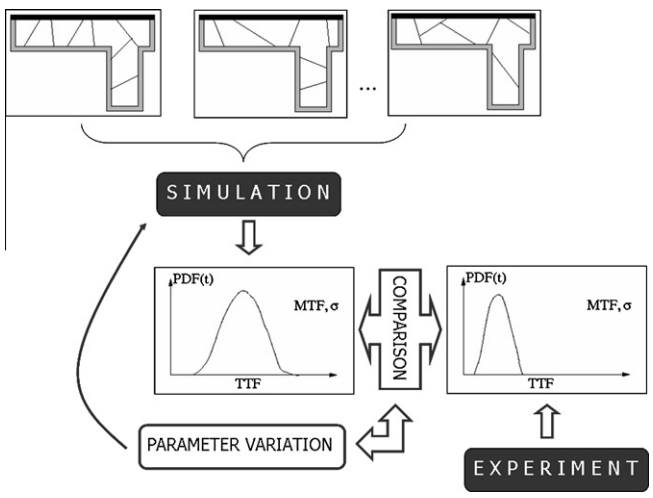

Fig. 10. Electromigration model calibration using a multitude of microstructural inputs.

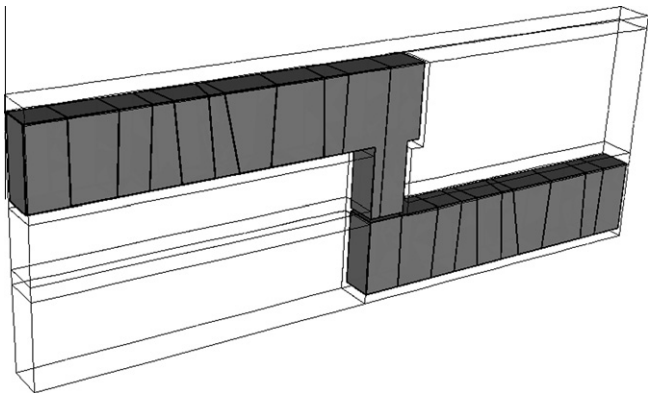

Fig. 11. Dual-damscene interconnect structure.

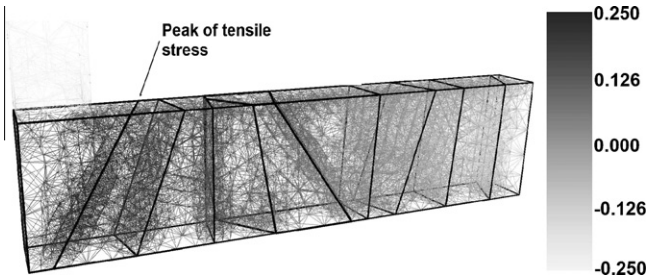

Fig. 13. Hydrostatic stress distribution in a simulated interconnect (in MPa). The peak value is located at grain boundaries, where vacancies are trapped.

generates a lognormal distribution of grain sizes. Then, following this distribution, the interconnect line is cut along its length by the planes which form the grain boundaries. Furthermore, the angles between the grain boundaries planes and the line surface follow a normal distribution with a median value of 90°. The corresponding standard deviation can also be specified.

In Fig. 10 we present the schema of the simulation procedure. Three standard deviations for the distribution of grain sizes are considered, namely 0.1, 0.3, and 0.6. For each of them 20 dual-damascene interconnect structures were created with the microstructure generation tool. As the interconnect line is assumed to present a bamboo structure, the median grain size is equal to the line width, 0.10 μm. The barrier, capping, and interlayer dielectric layers are Ta, SiN, and SiO_2, respectively. The corresponding interconnect structure is sketched in Fig. 11.

Fig. 12 shows the hydrostatic tensile stress development for the structures with grain size standard deviation of 0.3. The stress peak value follows the peak of the trapped vacancy concentration and is located at the intersection of grain boundaries with the capping layer, as shown by Fig. 13.

Collecting the times to failure from Fig. 12 and calculating the cumulative failure percentages results in the distributions of EM life times shown in Fig. 14. The life times are fitted by lognormal distributions. The obtained standard deviations are 0.0065, 0.0080, and 0.0085 for the grain size distributions with standard deviations of 0.1, 0.3, and 0.6, respectively. The standard deviations for the EM life times are very small compared to those frequently observed in experiments [5]. Several factors can explain this behavior. First, for convenience, we have used a small value of stress threshold as failure criterion to determine the interconnect life time. As can be seen from Fig. 12, the variation of the life times can be more pronounced for higher stress thresholds. Second, the simulation parameters and material properties are independent of the grain distribution. This means that the mechanical properties and diffusivities, are equal and constant for all grains in an interconnect line, for all simulated structures. This is clearly not the case in reality, as it is well known that the material properties vary according to the grain orientation. It is expected that the atomic diffusion along the copper/capping layer interface changes from grain to grain, inducing a flux divergence at the corresponding grain boundary. Moreover, the diffusivities are different from line to line as the grain distribution varies. Therefore, given the simplifications we have made, the small standard deviations obtained from our simulations should be expected.

Nevertheless, our results show that the grain distribution still affects the EM life time distribution. When the grain size distribution exhibits a smaller standard deviation, the corresponding interconnect lines have a more uniform distribution of the grains. As a consequence, the stress build-up has smaller variations yielding a smaller standard deviation of the EM life times. On the other hand, increasing the grain size standard deviation, the lines exhibit significant differences in the grain structures, which leads to increased variations for the stress development. Thus, a larger standard deviation of EM life times is expected. This behavior is presented in Fig. 15 which shows that the increase of the standard deviation of the distribution of grains sizes increases the standard deviation of the EM life time distribution.

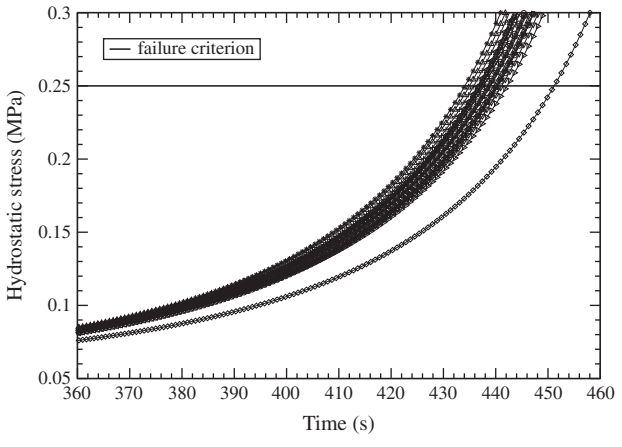

Fig. 12. Peak of hydrostatic stress development for the set with grain size standard deviation of 0.3.

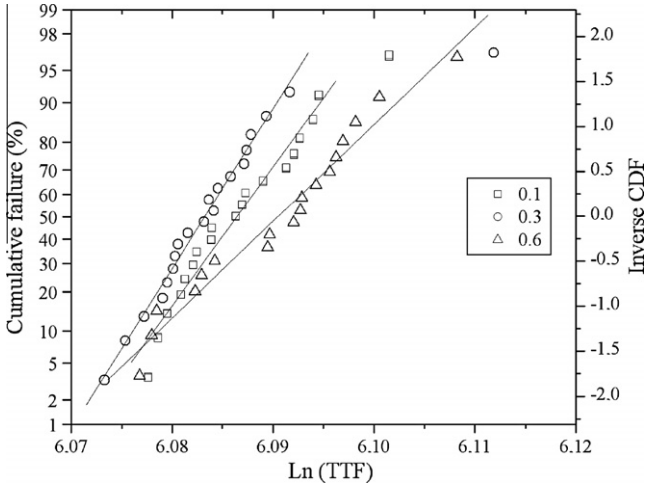

Fig. 14. Electromigration life time distributions.

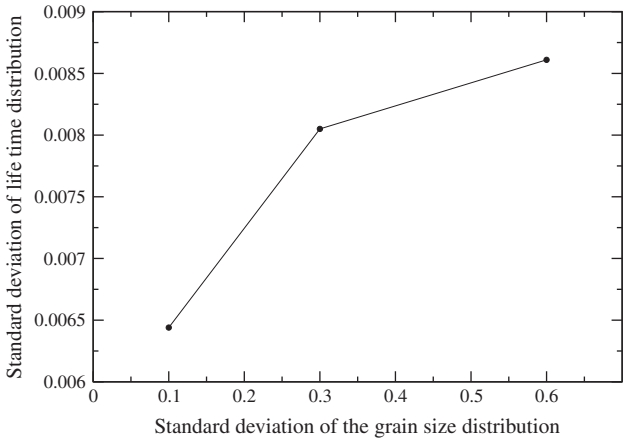

Fig. 15. Electromigration life time standard deviation for different standard deviations of grain size.

8. Conclusion

The importance of fast diffusivity paths for modern interconnect technologies is increasing. Crucial parameters, such as the effective valence in the fast diffusivity paths, are either not obtainable from experimental results or their determination is very unreliable. The quantum mechanical theory of EM offers a spectrum of methods for the calculation of the effective valence and some of them are presented in this work. Exact values of the effective valence are used for parametrization of continuum-level models which enable the simulation of EM behavior for long times. Void evolution including the influence of the fast diffusivity paths is simulated using a three-dimensional Level-Set method. The simulation results are successfully verified through comparison with experimental observations. Additionally, the impact of the microstructure statistics on EM failure time is analyzed.

Acknowledgment

Part of this work has been supported by the Austrian Science Fund with the Project P18825-N14.

References

[1] Hu C-K, Gignac L, Rosenberg R. Electromigration of Cu/low dielectric constant interconnects. Microelectron Reliab 2006;46:213–31.
[2] Tan CM, Roy A. Electromigration in ULSI interconnects. Mater Sci Eng 2007;58:1–75.
[3] Ryu C, Kwon K-W, Loke ALS, Lee H, Nogami T, Dubin VM, et al. Microstructure and reliability of copper interconnects. IEEE Trans Electron Dev 1999;46(6):1113–20.
[4] Lloyd J, Arzt E. A simple model for stress voiding in passivated thin film conductors. In: Symposium proceedings on materials reliability in microelectronics II, vol. 265; 1992. pp. 45–57.
[5] M. Hauschield, Statistical analysis of electromigration lifetimes and void evolution in Cu interconnects. Dissertation, The University of Texas at Austin; 2005.
[6] Ceric H, de Orio RL, Cervenka J, Selberherr S. A comprehensive TCAD approach for assessing electromigration reliability of modern interconnects. IEEE Trans Dev Mater Reliab 2009;9:9–19.
[7] Ceric H, de Orio RL, Cervenka J, Selberherr S. Stress-induced anisotropy of electromigration in copper interconnects, Stress-induced phenomena in metallization. AIP 2008:56–62.
[8] Ho PS, Kwok T. Electromigration in metals. Rep Prog Phys 1989;52:301–48.
[9] Bosvieux C, Friedel J. Sur L'electrolyse des Alliages Metalliques. J Phys Chem Solids 1962;23:123–36.
[10] Kumar P, Sorbello RS. Linear-response theory of the driving forces for electromigration. Thin Solid Films 1975;25:25–35.
[11] Sorbello RS. Pseudopotential-based theory on the driving forces for the electromigration in metals. J Phys Chem Solids 1973;34:937–50.
[12] Kresse G, Furthmüller J. Efficient iterative schemes for ab initio total-energy calculations using a plane-wave basis set. Phys Rev B 1996;54:11169–86.
[13] Sorbello RS. Theory of electromigration. Solid State Phys 1998;15:159–231.
[14] Sorbello RS. Microscopic driving forces for electromigration. Lloyd JR, Yost FG, Ho PS, editors. Materials reliability issues in microelectronics, vol. 225; 1996. p. 3–10.
[15] Gleixner RJ, Clemens BM, Nix WD. Void nucleation in passivated interconnect lines: effects of site geometries, interfaces, and interface flaws. J Mater Res 1997;12:2081–90.
[16] Fridline DR, Bower AF. Influence of anisotropic surface diffusivity on electromigration induced void migration and evolution. J Appl Phys 1999;85:3168–74.
[17] Sethian JA. Level set methods and fast marching methods: evolving interfaces in computational geometry, fluid mechanics, computer vision and materials science. Cambridge University Press; 1999.
[18] Rosenberg R, Ohring M. Void formation and growth during electromigration in thin films. J Appl Phys 1971;42:5671–9.
[19] Sukharev V, Zschech E, Nix WD. A model for electromigration-induced degradation mechanisms in dual-inlaid copper interconnects: effect of microstructure. J Appl Phys 2007;102:530501–14.
[20] Doyen L, Petitprez E, Waltz P, Federspiel X, Arnaud L, Wouters Y. Extensive analysis of resistance evolution due to electromigration-induced degradation. J Appl Phys 2008;104:123521–5.
[21] Suo Z, Wang W, Yang M. Electromigration instability: transgranular slits in interconnects. Appl Phys Lett 1994;64:1944–6.
[22] Mahadevan M, Bradley R. Simulations and theory of electromigration-induced slit formation in unpassivated single-crystal metal lines. Phys Rev B 1999;59:11037–46.
[23] Arzt E, Nix WD. A model for the effect of line width and mechanical strength on electromigration failure of interconnects with near-bamboo grain structures. J Mater Res 1991;6:731–6.